Article:
De Santis, A, Hanson, BC and Fairweather, M (2021) Hydrodynamics of annular centrifugal contactors: A CFD analysis using a novel multiphase flow modelling approach. Chemical Engineering Science, 242. 116729. p. 116729. ISSN: 0009-2509

https://doi.org/10.1016/j.ces.2021.116729

Hydrodynamics of Annular Centrifugal Contactors: a CFD analysis using a novel multiphase flow modelling approach

A. De Santis [a,*], *B. C. Hanson* [a], *M. Fairweather* [a]

[a] *School of Chemical and Process Engineering, University of Leeds, LS2 9JT, Leeds, United Kingdom*

Abstract

Annular Centrifugal Contactors (ACCs) are a promising process intensification technology for liquid-liquid extraction. Still, there is a limited understanding of the hydrodynamic conditions observed within ACCs and Computational Fluid Dynamics has the potential to shed light on this. However, the presence of a broad range of interfacial scales prevents the use of standard multiphase flow models. Therefore, a generalized multiphase modelling approach has been proposed, which allows for the simulation of multiscale multiphase flows. This approach has been applied to the simulation of a laboratory-scale ACC. It is demonstrated that the approach can provide information on the hydrodynamic behaviour of the system including hold-up, droplet size distribution and residence time; this, in turn, allows evaluation of the mass transfer performance. It is concluded that the modelling technique represents a valuable tool for gaining in-depth understanding of the hydrodynamics of ACCs, thus allowing for the prediction of their performance.

Keywords: Annular Centrifugal Contactors, Liquid-liquid extraction, Computational Fluid Dynamics, Multiphase flows

1. Introduction

Liquid-liquid extraction is a key process in current spent nuclear fuel reprocessing methods as well as in advanced reprocessing technologies foreseen for the next generation of nuclear power plants [1]. For instance, liquid-liquid extraction is used in the Plutonium Uranium Reduction Extraction (PUREX) process to separate and purify uranium and plutonium from each other and from fission products contained in irradiated uranium fuel elements [2]. Intensified liquid-liquid extraction, which is attained in devices such as pulsed sieve-plate extraction columns and Annular Centrifugal Contactors (ACCs), allows for higher extraction efficiencies and lower residence times compared to the standard extraction process taking place in devices such as mixer-settlers [3] [4].

In particular, ACCs are regarded as a promising technology due to their high mass transfer rates and good separation efficiency. However, they are characterised by a highly complex

* Corresponding author.
Email address: a.desantis@leeds.ac.uk
Tel: +44(0)113 343 2444

hydrodynamic behaviour and there is a general lack of understanding of the local features of the multiphase flow as well as of the local droplet size distribution found in these devices [5].

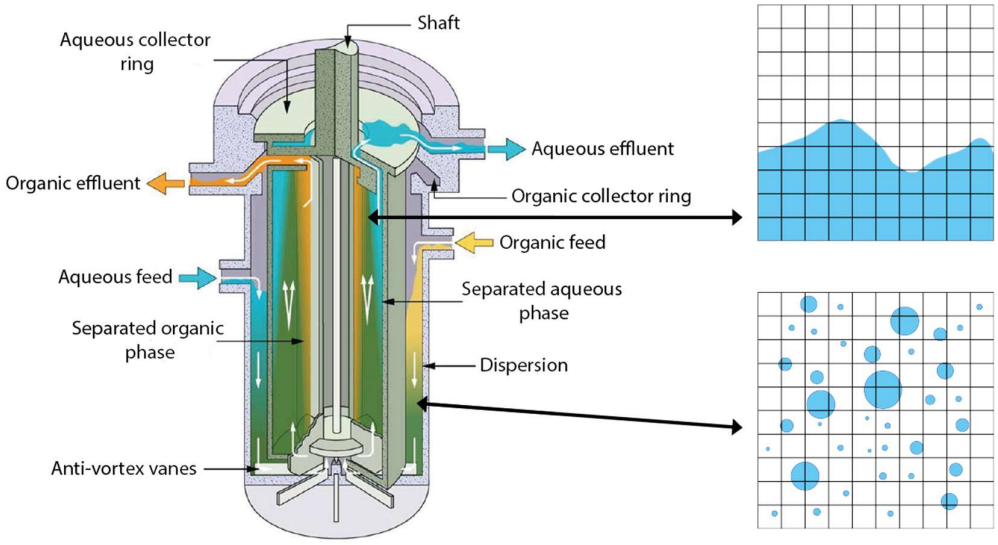

Figure 1. Schematic of an ACC (left) and qualitative representation of interface-resolving (top-right) and interface-averaging (bottom-right) approaches.

A schematic representation of an ACC is provided on the left-hand side of Figure 1. Both the aqueous and the organic phases enter the device in the mixing region, i.e. in the annular section encompassed by the outer case and the external rotor wall. Due to the high-speed rotation imparted by the rotor, the mixing region is dominated by a Taylor-Couette-type multiphase flow and the mixture inside the annulus is subject to high shear and turbulence. This results in the formation of a fine dispersion, which is highly desirable to enhance the mass transfer of the solute to the solvent. This finely dispersed mixture is collected at the bottom of the device and then guided within the rotor by means of dedicated vanes. Coalescence and phase separation take place by means of the different centrifugal force experienced by the two phases within the rotor due to their different density. At the top of the rotor, the two phases are collected and guided to their outlet sections by means of a complex weir system.

Computational Fluid Dynamics (CFD) has the potential to allow for in-silico investigation of ACCs and thus shed light on the intricate hydrodynamics of these devices. However, this is hindered by the complexity of the flow to be simulated; in particular, the presence of a broad range of interfacial scales within the system precludes the use of standard "off-the-shelf" modelling approaches for multiphase flows [6] [7]. Standard multiphase models stem from two modelling approaches [8] [9]:

- Interface-averaging approach
- Interface-resolving approach

The interface-averaging approach results in the so-called multifluid (or Eulerian) models; in these models it is assumed that scale separation exists between the continuous and the dispersed phases;

this allows for conditional volume averaging of the governing equations, and therefore in this approach the interface morphology is not directly resolved. All the phases within the system, which share the same pressure, are represented as interpenetrating continua and each phase has its own momentum equation. Due to the averaging procedure and consequent loss of information on the interface morphology, suitable closures are needed for the exchange of momentum, heat and mass at the interface.

The interface-resolving approach seeks to directly resolve the morphology of the interface between the phases; therefore, the numerical grid has to be fine enough to allow for an adequate resolution of the interface, which hinders the application of this approach to finely dispersed flows. Two main model classes stem from this approach: interface-tracking models which track the evolution of the interface in a Lagrangian fashion, and interface-capturing models which reconstruct the interface from a known indicator function. Interface-capturing models include both the Level Set [10] and the Volume of Fluid (VoF) [11] techniques; the latter technique, in particular, is generally numerically robust and widely used in the simulation of segregated multiphase flows, but tends to show some degree of interface smearing due to the numerical diffusion of the indicator function. Therefore, a special numerical treatment is required to counteract this "unphysical" smearing and to retain the sharpness of the interface.

From the description of the operating principles of ACCs, and as schematically shown in Figure 1, it follows that the interface-averaging approach is better suited for the simulation of the finely dispersed flow observed in the mixing region, whilst an interface-resolving approach is desirable for the simulation of the segregated flow found within the rotor. This highlights the problems encountered when trying to apply modelling paradigms suitable for "idealized" flow configurations, such as the fully dispersed and the large-scale/segregated interface assumptions, to "real-life" multiscale complex flows. This has been demonstrated in the context of liquid-liquid extraction in the recent LES/VoF simulation of a Pulsed Sieve-plate Extraction Column reported in [12]. It has been observed that an extremely fine mesh, associated with an unfeasible computational cost, would be required to resolve the single droplets within the system following an interface-resolving approach; including the effects of the presence of these droplets, on the other hand, is key for the correct representation of the hydrodynamic behaviour and of the mass transfer within the system. A previous study [6] came to the same conclusion following a LES/VoF investigation of the CINC-V2 ACC. Therefore, it is clear that there is a need for a generalized multiphase modelling approach capable of switching between some form of the two different modelling paradigms, interface-resolving and interface averaging, based on the local flow conditions and mesh resolution [9] [13] [14].

In this context, the University of Leeds has developed a novel GEneralized Multifluid Modelling Approach (GEMMA) [15]. This approach relies on the multifluid modelling framework for the solution of the governing equations (i.e. each phase retains its own momentum equation, and therefore suitable models are needed to account for the exchange of momentum between the different phases). In regions where the interfacial scales are small compared to the

size of the mesh, a standard multifluid formulation suitable for small/dispersed interfaces is used, whilst an ad-hoc multifluid formulation suitable for large/segregated interfaces is used in those regions were the mesh is sufficiently fine to resolve the interface; a local binary switch is used to decide the local model formulation as a function of the ratio between the interfacial scales and the mesh resolution on a numerical cell-by-cell basis. Including a dependency on the local mesh resolution is crucial since, in the modelling context, "small" and "large" interfacial scales are always defined with respect to the local mesh size. The status of the switch allows for the activation/deactivation of different terms and models in the governing equations such that a standard multifluid formulation is recovered in the regions of small/dispersed interfacial scales, whilst an ad-hoc multifluid formulation suitable for large/segregated interfaces is used in the regions where the local mesh size guarantees adequate resolution of the interfacial scales.

The paper presents work on the application of the GEMMA approach to the simulation of the hydrodynamic behaviour of ACCs. An in-depth description of the modelling approach is given in Section 2. Section 3 reports the application of the modelling approach to the simulation of liquid-liquid extraction processes in ACCs: the numerical settings used in the different simulations are illustrated in Section 3.1, followed by the simulation of the mixing region of an ACC described in Section 3.2. The simulation of a laboratory-scale ACC is presented in Section 3.3, and a possible strategy for the application of the CFD results to the prediction of the mass transfer performance of the device is illustrated in Section 3.4. Finally, conclusions and future work are discussed in Section 4.

2. Modelling approach

The GEMMA approach has been implemented in the well-known open-source CFD code OpenFOAM v7.0 [16] [17]. The implementation is based on the built-in solver *reactingMultiphaseEulerFoam*, which is a standard multifluid solver for n compressible phases and can account for both heat and mass transfer. The solver also includes a broad variety of models for the interfacial transfer of momentum, heat and mass and can be coupled to an inhomogeneous population balance [18] to evaluate the local size distribution of the dispersed phase.

The GEMMA approach has been built on top of the standard multifluid modelling framework given by *reactingMultiphaseEulerFoam*. The key concept behind the GEMMA approach is the use of a suitable multifluid formulation based on the local interfacial morphology, i.e. large/segregated or small/dispersed; the local model formulation is decided via the introduction of a local binary switch C_α [14] [19]; the logic controlling the local switch status is reported in the flow-chart in Figure 2 an described in further detail below.

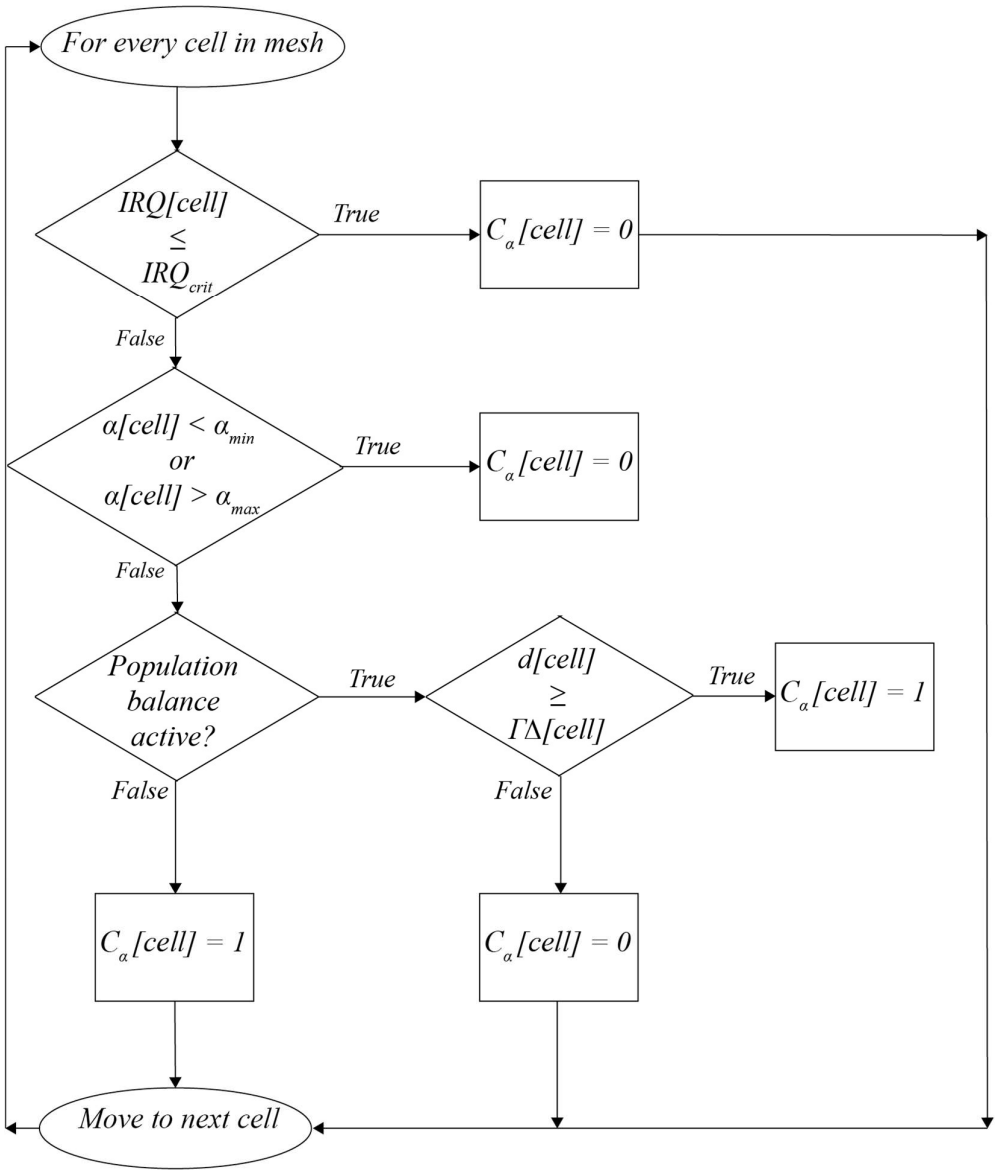

Figure 2: Flow-chart for the switch logic within GEMMA, reproduced with permission from [15].

In the cells of the numerical mesh in which C_α is equal to zero the GEMMA approach reduces to a standard multifluid approach suitable for small interfacial scales. In the cells where C_α is equal to one a multifluid formulation suitable for large interfacial scales is activated. In the numerical modelling context, it is important to underline that the concept of "small" and "large" interfacial scales is relative to the local size of the numerical grid. Therefore, the logic controlling the status of the switch is based on the capability of the local mesh resolution to resolve the local interfacial scales adequately; within GEMMA the user has the capability to specify the minimum resolution of the interface that has to been guaranteed to activate the large interfacial scales formulation. This is achieved by introducing the concept of an Interface Resolution Quality (IRQ) index [20]. IRQ is defined as:

$$IRQ = \frac{2}{\Delta\kappa} \quad \textbf{(1)}$$

where Δ is the local mesh size, which is evaluated as the cube root of the local cell volume, and κ is the local interface curvature, which is evaluated from the resolved volume fraction field. For a spherical dispersed phase element, $\kappa = 1/r$ and therefore $IRQ = {}^{2r}/_{\Delta} = d/\Delta$. A high value of IRQ corresponds to an accurate spatial resolution of the curvature of the interface. Within the switch logic, a user-specified critical value IRQ_{crit} is used control the desired level of resolution of the interface curvature necessary to activate the large-interface mode of the solver locally. A second switching criterion is used in combination with IRQ when the local dispersed phase size is known, for example, via the resolution of a population balance equation. In this logic, Γ is a parameter that allows control of the minimum number of cells needed to resolve the interfacial scales associated with a Dispersed Phase Element (DPE) of diameter d. This criterion activates the large interface switch in the cells where the local dispersed phase diameter is at least Γ times larger than the local mesh size.

Assuming incompressible phases, and neglecting heat and mass transfer, the momentum conservation equation for phase k in the multifluid formulation is given by:

$$\begin{aligned} \frac{\partial \alpha_k \boldsymbol{u_k}}{\partial t} + \nabla \cdot (\alpha_k \boldsymbol{u_k} \boldsymbol{u_k}) \\ = -\alpha_k \nabla p/\rho_k + \nabla \cdot (\nu_k \alpha_k \nabla \boldsymbol{u_k}) + \alpha_k \boldsymbol{g} \\ + \left(\boldsymbol{F_k} + \boldsymbol{F_{st,k}}\right)/\rho_k \end{aligned} \quad \textbf{(2)}$$

where the interfacial momentum exchange term $\boldsymbol{F_k}$ includes forces due to drag, lift, wall lubrication and turbulent dispersion; all these terms need suitable models in order to close the equation. The surface tension force $\boldsymbol{F_{st,k}}$ is usually taken equal to zero in the standard multifluid formulation developed in the context of small/dispersed interfaces.

The corresponding continuity equation for phase k reads:

$$\frac{\partial \alpha_k}{\partial t} + \nabla \cdot (\alpha_k \boldsymbol{u_k}) = 0 \quad \textbf{(3)}$$

In the cells in which the model is operating in large/segregated interface mode the local mesh resolution is theoretically fine enough to guarantee an adequate resolution of the morphology of the interface; therefore, it is desirable to maintain a "sharp" interface in these cells, similarly to what is done in interface-capturing models such as VoF. Within GEMMA, this is achieved by including a compressive term in the continuity Equation (3), following a technique commonly employed in the VoF approach to guarantee a sharp interface. Therefore, the continuity equation for phase k used in GEMMA reads:

$$\frac{\partial \alpha_k}{\partial t} + \nabla \cdot (\alpha_k \boldsymbol{u_k}) + \nabla \cdot \left(\boldsymbol{u_c} \alpha_k (1 - \alpha_k)\right) = 0 \quad \textbf{(4)}$$

where the term $\alpha_k(1 - \alpha_k)$ ensures that the compressive term is only active in the interface region and $\boldsymbol{u_c}$ is the compressive velocity. It has to be pointed out that the compressive term appearing in Equation (4) does not corresponds to any actual physical phenomenon, but is merely a numerical expedient used to counteract another purely numerical effect, i.e. the "smearing" of the interface [21].

The compressive velocity is evaluated as:

$$\boldsymbol{u_c} = C_\alpha |\boldsymbol{u}| \frac{\nabla \alpha}{|\nabla \alpha|} \quad \textbf{(5)}$$

where $\frac{\nabla \alpha}{|\nabla \alpha|}$ ensured that $\boldsymbol{u_c}$ is normal to the interface, and $|\boldsymbol{u}|$ is the magnitude of the relative velocity between the two phases at the interface. The binary switch C_α in Equation (5) ensures that the compressive term is only active in the large/segregated interface cells, whilst the standard multifluid continuity Equation (4) is recovered in the small/dispersed interface cells where C_α is equal to zero.

In order to develop a multifluid formulation suitable for large/segregated interfaces it has to be observed that the standard interfacial momentum exchange closures, which have been developed under the assumption of the presence of a dispersed phase made up of DPEs such as droplets or bubbles, are not applicable in large/segregated interface cells. Therefore, a closure for the interfacial momentum exchange due to drag in the presence of large/segregated interfaces [9] is used within GEMMA in the cells where C_α is equal to one; all the other interfacial momentum exchange terms are neglected in those cells. A novel generalized blending technique, depending on the local C_α value, is used to blend between interfacial exchange models suitable for small and large interfacial scales [15].

In addition, the resolution of the interfacial morphology in the regions of large/segregated interfacial scales allows for the evaluation of the surface tension force. A multifluid version [22] of the Continuum Surface Force (CSF) [23] [24] is employed to evaluate the surface tension force $\boldsymbol{F_{st,k}}$ in the cells where C_α is equal to one. The surface tension force within GEMMA is therefore evaluated as:

$$\boldsymbol{F_{st,k}} = \alpha_k \sum_{i=1}^{n_k} \left(C_{\alpha_{k,i}} \sigma_{k,i} \kappa \nabla \alpha \frac{2\rho}{\Delta \rho_{k,i}} \right) \quad \textbf{(6)}$$

where $\sigma_{k,i}$ is the surface tension force coefficient between phases i and k, and ρ is the density of the mixture, $\Delta \rho_{k,i}$. The interface curvature κ is evaluated on a smoothed volume fraction field, following the Smoothed Continuum Surface Force (SCSF) approach of [25].

From the discussion above, it follows that the multifluid formulation for large interfacial scales used within GEMMA in the cells where C_α is equal to one is based on three main features:

1. Introduction of a compression term in the continuity equation to guarantee a sharp interface
2. Introduction of a drag closure suitable for large/segregated interfacial morphologies and of a generalized blending method between closures suitable for small/dispersed and large/segregated interfacial scales
3. Introduction of a multifluid version of the SCSF for the evaluation of the surface tension force.

The GEMMA formulation described above has been tested in different test cases in [15], where it has been shown to be as accurate as standard interface-capturing models in the simulation of cases characterized by large/segregated interfaces, whilst a standard multifluid formulation is

recovered in cases characterized by small/dispersed interfaces. In the same work the authors also demonstrated the capability of the GEMMA approach to deal with a prototypical multiscale flow, i.e. a water jet plunging into a quiescent pool [26].

2.1 Reduced population balance

In the context of the simulation of liquid-liquid extraction processes, a knowledge of the droplet size distribution in the mixing region is key for the hydrodynamic characterisation of ACCs and also for the evaluation of their performance in terms of mass transfer. A population balance approach can be used within GEMMA to evaluate the DPE size distribution when working in dispersed-interface mode. The formulation of GEMMA is fully compatible with the MUSIG [18] multigroup inhomogeneous population balance embedded within the *reactingMultiphaseEulerFoam* solver in OpenFOAM, which allows for the evaluation of the DPEs diameter distribution.

However, in order to reduce the computational overhead associated with the resolution of the population balance equation, a reduced population balance has been implemented within GEMMA as an alternative to MUSIG. The reduced population balance is based on the One Primary One Secondary Particle Method (OPOSPM) [27], which is a special instance of the Sectional Quadrature Method of Moments (SQMOM) in which only one primary particle and one secondary particle are considered [27] [28]. In the OPOSPM approach two low-order moments can be conserved, and the secondary particle represents a Lagrangian fluid particle carrying information about the droplet population through its low-order moments. Although the selection of these moments is arbitrary, the total number and volume concentrations are the most natural candidates for the conservation of the total number and mass of the DPEs. Because the total number and volume concentrations are conserved, the population density is represented by a single particle (assumed to have a spherical shape) whose size is characterised by the diameter:

$$d_{30} = \sqrt[3]{\frac{m_3}{m_0}} = \sqrt[3]{\frac{6\alpha_d}{\pi N_d}} \tag{7}$$

where α_d and N_d are the volume fraction and the particle number density of the dispersed phase, respectively, which are related to the zeroth and third moment of the distribution m_0 and m_3. The dispersed phase volume fraction is already known from the solution of the related continuity equation, so the OPOSPM only requires the solution of one additional conservation equation for N_d, which reads:

$$\frac{\partial(\rho_d N_d)}{\partial t} + \nabla \cdot (\rho_d \boldsymbol{u_d} N_d) = \rho_d S \tag{8}$$

where the source term is given by:

$$S = (N_d - 1) g(d_{30}) - \frac{1}{2} a(d_{30}, d_{30}) N_d^2 \tag{9}$$

In the equation above, $g(d_{30})$ and $a(d_{30}, d_{30})$ represent the break-up and coalescence rates, respectively, which have to be evaluated by using a suitable closure. In all the cases considered in this paper, the break-up model of [29] and the coalescence model of [30] have been used.

The OPOSPM population balance allows for the evaluation of d_{30}; mathematically, this is a more coherent choice compared to d_{32}, since the former is a natural quadrature node whilst the latter is not. However, keeping in mind the importance of evaluating the interfacial area density a_i to assess mass transfer within the device, it is worth observing that knowledge of d_{32} allows evaluation of the interfacial area density as:

$$a_i = \frac{6\alpha}{d_{32}} \tag{10}$$

For the simulation of ACCs, [14] proposed to use the knowledge of d_{30} directly available from the OPOSPM population balance and estimate the ratio of d_{30}/d_{32}, which for liquid-liquid dispersions in centrifugal contactors is observed to be consistently in the range 0.75-0.8. A value of 0.76 is used throughout the simulations presented in this work.

3. Simulation of liquid-liquid extraction processes

The section presents the results obtained using the GEMMA approach for the simulation of two cases relevant to liquid-liquid extraction processes in ACCs: firstly, the multiphase flow observed in the annular section of an ACC has been investigated, in order to assess the capabilities of the modelling approach in the simulation of the mixing region of ACCs and validate the numerical results against available experimental observations. Secondly, a laboratory-scale ACC has been simulated, in order to demonstrate the capability of GEMMA to predict the complex flow-field observed in these devices and to yield key information on their hydrodynamic behaviour.

3.1 Numerical set-up

All the simulations were performed using the open-source CFD code OpenFOAM v7.0. Second-order Total Variation Diminishing (TVD) schemes were used for the spatial discretization of the convective term in all the transport equations, whilst a first-order Eulerian scheme was used to discretize the temporal derivative terms. The semi-implicit MULtidimensional limiter for Explicit Solution (MULES) was used to guarantee the boundedness of the volume fraction fields [21]. The pressure-velocity coupling algorithm employed in all the simulation was a multiphase extension of the PIMPLE algorithm [16]. The time-step size employed in all the simulations enforced a maximum Courant number value equal to 0.5.

3.2 Simulation of the mixing region of an ACC

In order to assess the capability of the GEMMA approach with respect to the simulation of the annular mixing section of an ACC, the flow in the mixing region of the CINC-V2 centrifugal contactor at different rotor speeds was simulated. This contactor has been investigated experimentally in [31]. The computational domain employed for the present simulations was based on the work of [14] and consists of a 5° wedge, representing the annular region between the casing and the outer rotor wall of the contactor, with periodic conditions enforced on the wedge sides. The domain was discretized in space with a structured hexahedral mesh of size equal to 0.4 mm, which resulted in a cell count of 19,600. For the baseline case, corresponding to a rotating speed of 2000 RPM, a more refined mesh of size equal to 0.2 mm (corresponding to a cell count of about 160k) was also used to assess the sensitivity of the results to mesh resolution. All the simulations were run for a physical time of 3 seconds, except for the cases at rotating speeds of 1100 and 1500 RPM, for which 6 seconds of physical time were simulated.

All the simulations were initialized with three horizontal layers of water, organic phase (PDMS) and air with a height ratio of 3/1/3. The air phase was considered to be laminar, whilst a Large Eddy Simulation (LES) approach with a dynamic Smagorinsky [32] [33] closure for the subgrid-scale stresses was used for both the water and the PDMS phases; additionally, a wall function [34] was used to relax the mesh size requirements at the wall, thus resulting in a wall-modelled LES approach. The GEMMA approach was used to simulate the dispersion of the organic phase in water, whilst it was assumed that a sharp interface was maintained between the air and the two liquid phases at all times, and hence a uniform value of C_α = 1 was imposed for the air-liquid interfaces. The OPOSPM population balance approach was used to estimate the PDMS droplet size. This allowed for the use of the switching logic based on both IRQ and the dispersed phase diameter for the evaluation of the local value of C_α. The values for both IRQ_{crit} and Γ were taken equal to 2. Even though these values correspond to a coarse resolution of the interface curvature and of the dispersed droplets, this choice was made deliberately to demonstrate to capability of GEMMA to switch between large-interface and small/dispersed-interface modes in the considered flow configuration.

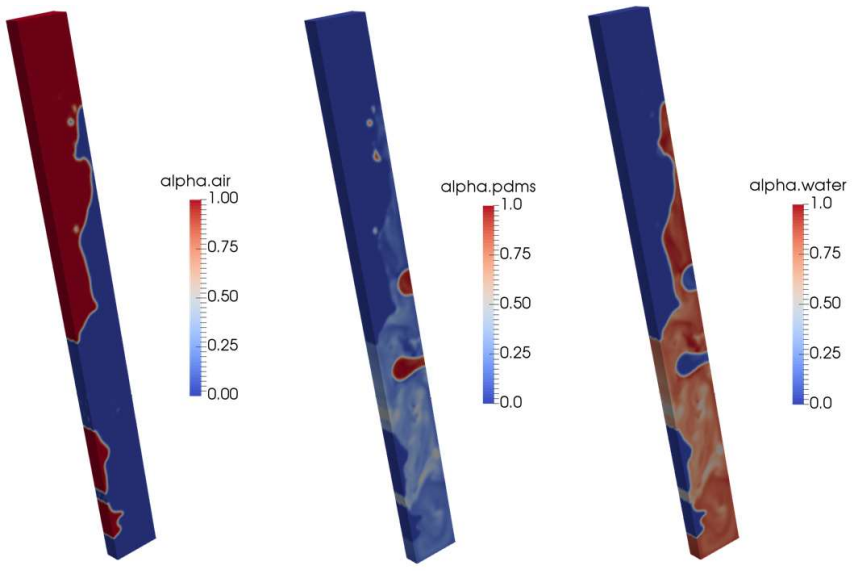

Figure 3. Instantaneous contours of air, PDMS and water volume fraction on the fine mesh.

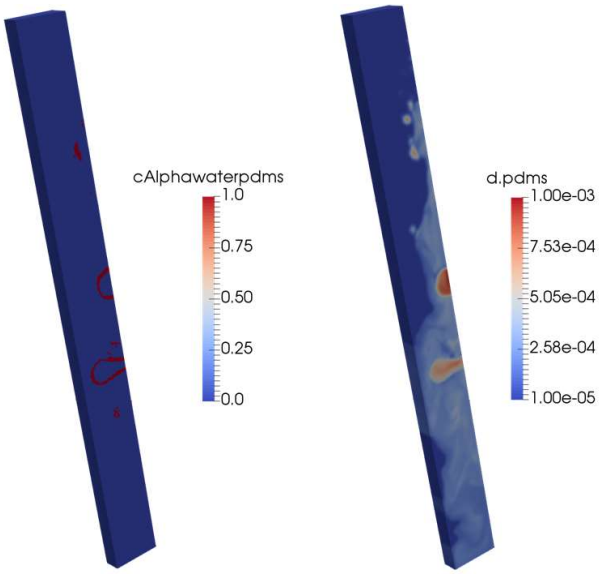

Figure 4. Instantaneous contours of water-PDMS $\boldsymbol{C_\alpha}$ and PDMS diameter (m) on the fine mesh.

A snapshot of the instantaneous volume fractions of the three phases at $t = 0.7\ s$ on the fine mesh for the baseline 2000 RPM rotating speed is shown in Figure 3. It can be seen that the model keeps a sharp interface between air and the two liquid phases everywhere in the domain due to the uniform unitary value of C_α. For water and PDMS, on the other hand, the model works in interface-averaging mode almost everywhere, and this is due to the fine dispersion of PDMS in water induced by the rotation of the rotor. The corresponding contours for C_α and the PDMS diameter predicted by the reduced population balance are shown in Figure 4. It can be seen how the small PDMS diameter compared to the mesh size results in C_α being zero almost everywhere

in the domain, and hence in the interface-averaging behaviour shown in Figure 3. The only exception is represented by two pockets of entrained dispersed phase, for which the mesh is fine enough to switch to C_α = 1, which guarantees the sharp interface observed in Figure 3 for these two features.

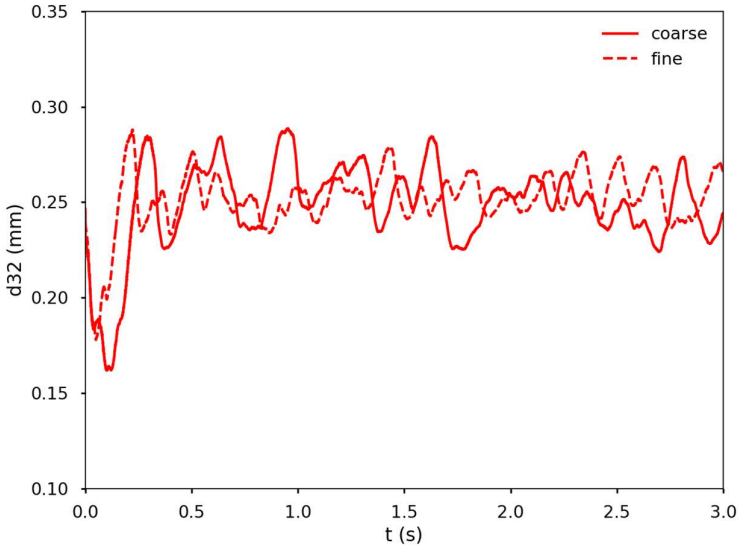

Figure 5. Transient evolution of the liquid-averaged PDMS diameter on the coarse and fine meshes at 2000 RPM.

The variation of the liquid-averaged PDMS diameter over time for the baseline 2000 RPM case is shown in Figure 5. The two meshes show similar trends for this quantity, with time-averaged values of 248 and 252 μm for the coarse and the fine meshes, respectively, compared to an experimental value of 361 μm; thus, all the simulations at different RPM values were performed on the coarse mesh only. Also, when performing a quantitative comparison between the experimental and the numerical results for this quantity, one should keep in mind that the experiments were performed on the actual contactor, whilst the numerical simulations are based on a simplified geometry of the annular region only.

A comparison between the experimental and numerical values of the liquid-averaged Sauter mean diameter d_{32} is shown in Figure 6. The average Sauter mean diameter is expected to decrease following a power-law trend with increasing rotating speeds and, overall, this is the case in both the experimental and the numerical results. However, some experimental points are observed to deviate from the expected power-law curve. This is likely due to the specific technique used in [31] to calculate d_{32} from the droplet size distribution, since the mean diameter values reported in the same work do not show any deviation from the expected power-law curve. From Figure 6, it can be observed that the numerical results are in an overall good agreement with the experiments, especially at the higher rotating speeds. At lower rotation speeds the discrepancy between the numerical results and the experimental measurements is more significant. In this respect, it should be kept in mind that the droplet size distribution gets broader at lower rotation

speeds, which results in a higher standard deviation associated with the values reported at such speeds [31]. Overall, these results are seen as an encouraging demonstration of the ability of GEMMA coupled with an OPOSPM population balance to predict the complex multiphase flow behaviour observed in the mixing region of ACCs and to provide a good prediction of the dispersed phase diameter.

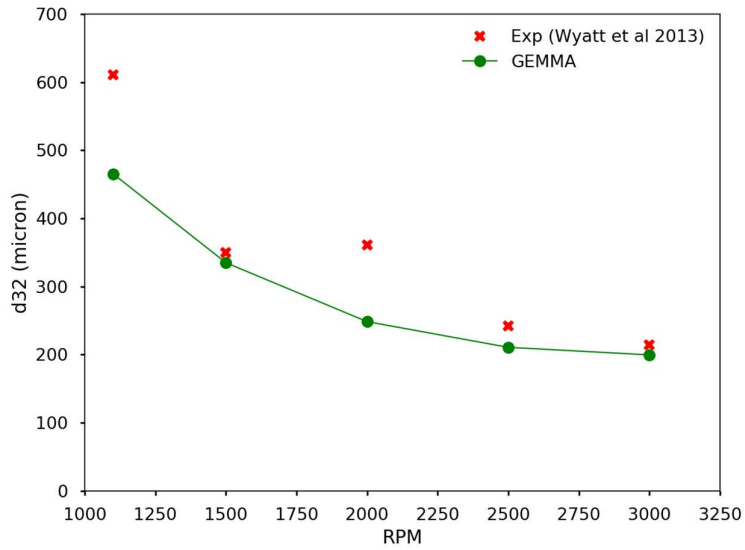

Figure 6. Measured and calculated time-averaged PDMS diameter at different rotating speeds.

3.3 Simulation of a laboratory-scale ACC

The previous section has shown the capability of the GEMMA concept to predict the flow field observed in the annular section of an ACC. This section describes the application of the modelling concept to the flow in a complete laboratory-scale ACC. The design of this device does not replicate any specific existing ACC, as this exercise is meant to be a proof of concept to assess the capabilities of GEMMA in the simulation of a generic "realistic" laboratory-scale device. In this respect, it should also be noted that no experimental data are currently available that permit a thorough validation of a CFD simulation of a complete ACC; for instance, the experiments in [31] have been performed in a complete ACC, but only the flow observed in the annular section of the device has been characterised experimentally. For this reason, and also due to the simplifying assumptions that are addressed below, the numerical results obtained in this simulation are not directly compared against any experimental data.

The computational domain is depicted in Figure 7. The outer diameter of the ACC is equal to 6.3 cm. The inner diameter of the annulus and the inner diameter of the rotor are equal to 5.4 and 5.0 cm, respectively. The height of the ACC is equal to 8.2 cm. The diameter of the inlet pipes is equal to 0.8 cm. Four radial vanes are present at the bottom of the device to drive the mixture within the rotor. A X-shaped stirrer is attached to the shaft within the rotor. The domain is

discretised using a cut-cell mesh, shown in a vertical mid-plane section in Figure 7, consisting of 2.2M hexahedral cells.

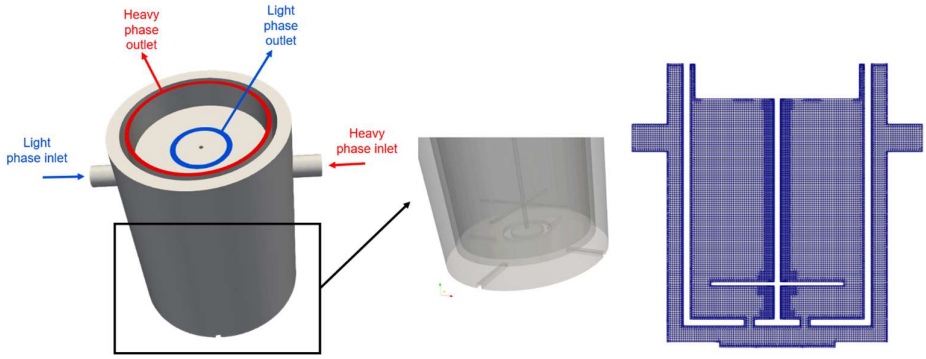

Figure 7. Computational domain and numerical grid for the laboratory-scale ACC simulation.

With respect to a "real" ACC, the two main simplifying assumptions made in the present simulation are:

1. The complex outlet weir systems are not included in the computational domain. Instead two annular outlet sections are imposed for the heavy phase (shown in red in Figure 7) and the light phase (shown in blue in Figure 7). An additional pressure overhead equal to 3000 Pa is imposed at the heavy phase outlet to account for the presence of the weir system that is not included in the computational model.
2. The presence of the air phase is neglected in the simulation; the ACC is modelled as a two-phase system.

A tributyl phosphate (TBP)/dodecane mixture at 30/70 wt% and a 3 M nitric acid (HNO_3) solution are assumed to represent the light organic phase and the heavy aqueous phase, respectively. The physical properties of the two phases are reported in Table 1. The aqueous over organic volumetric flow rate ratio is equal to 2:1. The rotating speed of the rotor is equal to 3600 RPM. The Moving Reference Frame (MRF) approach is used to account for the rotation in the numerical simulation.

Table 1. Physical properties of the working fluids.

	Density (kg m^{-3})	**Dynamic viscosity (Pa s)**
TBP/dodecane	806	1.894×10^{-3}
Nitric acid	1110	1.129×10^{-3}
Surface tension (N m^{-1})	0.00983	

Both TBP/dodecane and nitric acid were considered to be turbulent, and the wall-modelled LES approach with the dynamic Smagorinsky closure for the subgrid-scale stresses described in Section 3.2 was used for both phases. The diameter of the TBP/dodecane phase was evaluated using the OPOSPM population balance.

For the simulations, after an initial transient of 6 seconds, the flow in the system was observed to have reached a statistically-steady state. After this initial transient period, flow statistics were collected for 4 seconds, leading to a total of 10 seconds of simulated flow time.

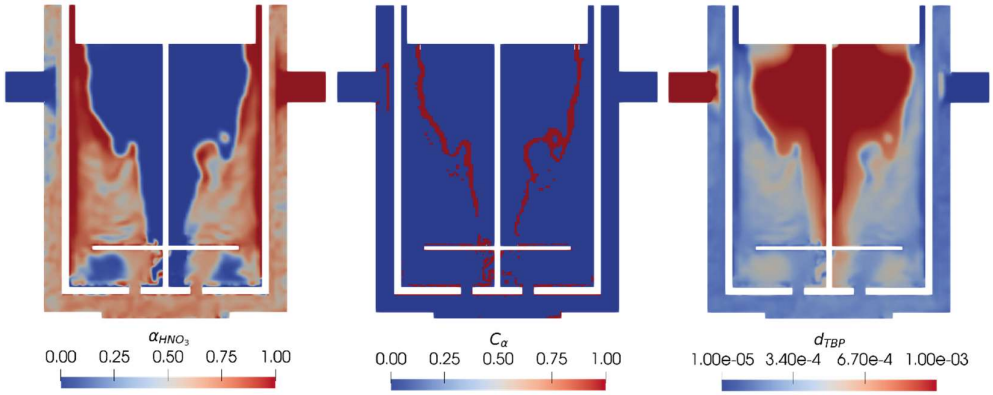

Figure 8. Instantaneous contours (t = 7.5 s) of HNO3 volume fraction, $\boldsymbol{C_\alpha}$ switch and diameter of the dispersed phase (m) on the ACC mid-plane.

The instantaneous contours of the heavy phase volume fraction, C_α switch and light phase diameter on the ACC vertical mid-plane evaluated at $t = 7.5\,s$ are shown in Figure 8. The instantaneous HNO_3 contours within the annulus show that any information on the interface morphology is lost, and this is due to the fact that the model is working in small/dispersed-interface mode in that region. This is confirmed by the C_α contour plot, which shows that the switch is set to zero almost everywhere within the annulus. Moving to the rotor region, it can be seen that due to coalescence of the organic phase and the consequent increase in the diameter of the dispersed phase, the C_α switch tends to assume a unity value at the interface between the two phases; this is particularly evident in the upper part of the rotor region, where the cone-shaped interface typical of ACCs [5] can be observed and complete phase separation is achieved. The activation of the C_α switch within the rotor region allows the model to work in large-interface mode; this results in a direct resolution of the interface morphology, as can be inferred by the sharp interface shown in the α_{HN_3} contour plots in the upper part of rotor region, and therefore in an accurate location of the dispersion band. The capability of GEMMA to handle the transition from the unresolved small interfacial scales within the annulus to the large segregated interface found in the rotor region is key to the accurate characterization of the hydrodynamic behaviour of the ACC. With respect to the organic phase diameter, it should be pointed out that the contours shown in Figure 8 report the diameter obtained from the OPOSPM population balance; although this diameter is defined in every cell of the computational domain, it is only representative of the interfacial scales in the regions where C_α is equal to zero. In these cells the interfacial morphology is not directly resolved and the interfacial area density can be evaluated from the Sauter mean diameter given by the population balance via Equation (9).

In the large-interface cells, the interfacial morphology is directly resolved and therefore the interfacial scales should be evaluated directly from the volume fraction field. In these cells Equation (9) is no longer representative of the interfacial area density, which can be evaluated as:

$$a_i = |\nabla \alpha| \tag{11}$$

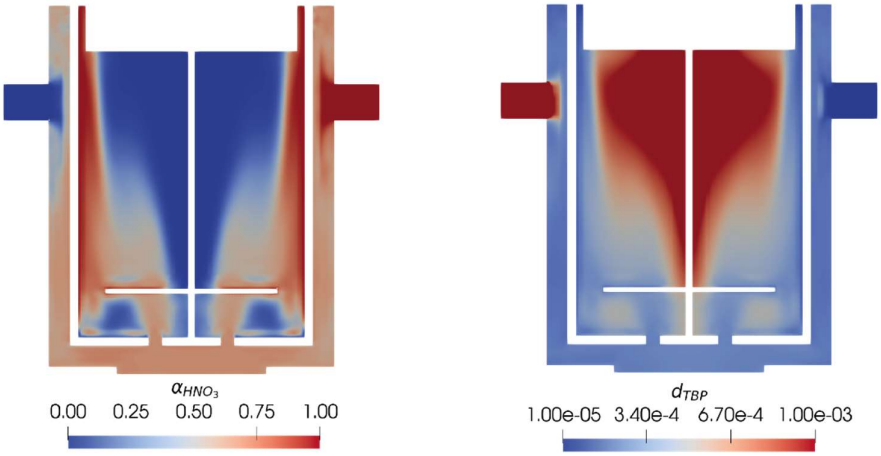

Figure 9. Time-averaged contours of HNO_3 volume fraction and TBP/dodecane phase diameter on the ACC mid-plane.

Figure 9 shows the time-averaged contours of the HNO_3 volume fraction and of the TBP/dodecane phase diameter. From the time-averaged heavy phase volume fraction contours, it is observed that a fine dispersion is established within the annulus, as confirmed by the time-averaged diameter contours; within the rotor region, due to coalescence and separation, a cone-shaped interface is observed, with a well-defined dispersion band located between the heavy phase and the light phase outlets, and a complete disengagement of the two phases at the top of the rotor region.

The evolution of the organic phase hold-up over time is shown in Figure 10. It can be observed that the hold-up has reached a statistically steady-state in both the annulus and the rotor region at the start of the sampling period at t = 6 seconds. The time-averaged hold-up values are equal to 0.335 and 0.665 in the annulus and in the rotor region, respectively; it should be pointed out that the hold-up value within the rotor is affected by the absence of the entrained air in the simulation; in the actual operation of an ACC, an air cone is formed within the rotor and thus the hold-up value is expected to be less that the value observed in the present simulation.

Figure 11 shows the evolution of the spatially-averaged organic phase diameter within the annulus over time. It can be observed that this quantity also shows a statistically steady-state behaviour over the sampling period. The time-averaged diameter value in the annulus is equal to 0.170 mm. For comparison, the mean diameter evaluated with the correlation proposed by [35] is 0.243 mm. The correlation is given as:

$$\frac{d}{g} = 150(We)^{-0.65}(Re)^{-0.2}\left(\frac{\mu_d}{\mu_c}\right)^{0.5}\left(\frac{g}{D_i}\right)^{0.5} \tag{12}$$

where We and Re are the droplet Weber and Reynolds number, respectively, D_i is the inner diameter of the annulus and g is the annulus gap.

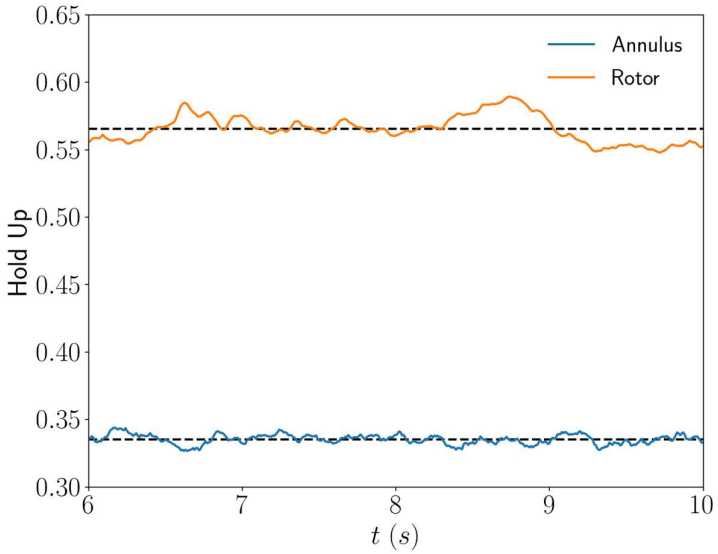

Figure 10. Transient evolution of the organic phase hold-up in the annulus and in the rotor region.

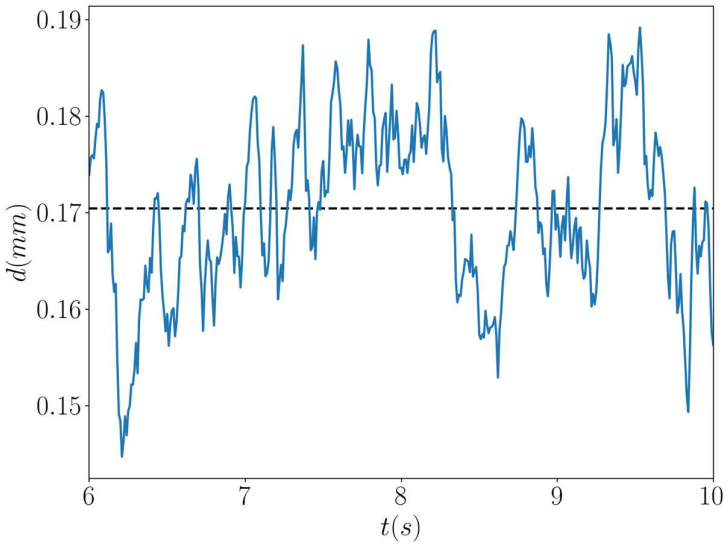

Figure 11. Transient evolution of the average organic phase diameter in the annulus.

The instantaneous organic phase droplet size distribution within the annulus at $t = 7.5\ s$ is shown in Figure 12. The spatially-averaged instantaneous diameter is equal to 0.175 mm at the considered time. The diameter distribution shape is in qualitative good agreement with the distributions that have been observed experimentally in ACCs [31], which confirms the ability of

the GEMMA approach coupled with OPOSPM to provide a reliable prediction of the expected droplet size distribution observed in the mixing section of ACCs.

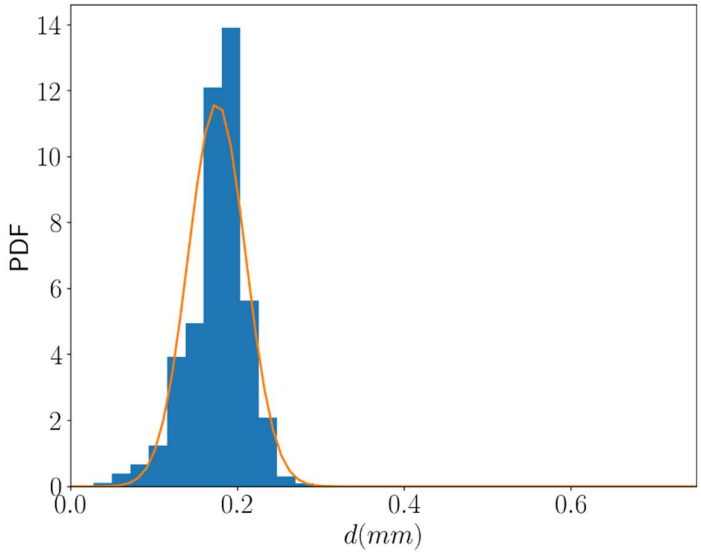

Figure 12. Instantaneous droplet size distribution within the annulus at t=7.5 s.

The residence time is a key parameter for the characterization of the performance of ACCs; in particular, the residence time of the organic phase within the annular mixing region is a key parameter for the evaluation of mass transfer within the device [5] [36]. Since the GEMMA approach allows for an accurate evaluation of the flow within ACCs, the resulting flow field can be used to evaluate the residence time associated with the given operating conditions.

For the operating conditions considered in the present simulation, the "plug-flow" residence time in the system is equal to 1.17 seconds. The "plug-flow" residence time is evaluated as:

$$t_{PF} = \frac{V}{\dot{Q}} \tag{13}$$

where V is the volume of the system and $\dot{Q}$ is the total volumetric flow rate through the inlets. The "plug-flow" residence time associated with the annular mixing region only is equal to 0.48 s.

However, it should be noted that idealized plug-flow and batch reactors are the only systems for which all the molecules of the working fluid will spend the same amount of time within the system [37] and can thus be characterised by a single value of the residence time. For non-idealized systems the concept of Residence Time Distribution (RTD) $E(t)$ is more appropriate [38]. Usually, the RTD is evaluated experimentally by injecting an inert fluid, i.e. a tracer, within the system and monitoring its concentration over time $C(t)$ at the outlet. From a CFD perspective, the equivalent of the aforementioned technique is to inject a passive scalar inside the system and track its evolution using an advection equation. In this work the focus is on the residence time of the dispersed organic phase, therefore the passive scalar used as a tracer has the same physical properties as the organic phase and the advective velocity field is given by the velocity associated with the continuous aqueous phase. For a step-shaped tracer injection, the RTD can then be evaluated as [37]:

$$E(t) = \frac{dC(t)}{dt} \tag{14}$$

Figure 13 shows the resulting outlet concentration and RTD for the passive scalar. It can be seen that the RTD for a passive scalar having the same physical properties as the organic phase is relatively narrow, with an average value of 1.19 seconds, which is very close to the residence time evaluated with a "plug-flow" assumption. Likewise, the average residence time of the passive scalar in the annular region is equal to 0.49 seconds, which is very similar to the value of 0.48 seconds obtained with a "plug-flow" calculation.

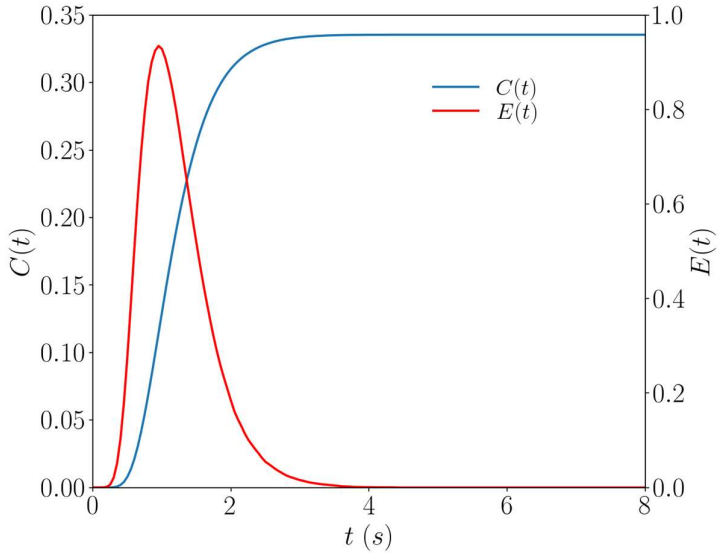

Figure 13. Exit age and RTD of a passive scalar advected by the aqueous phase through the system.

However, it should be noted that a passive scalar is unlikely to be representative of the RTD within the system for a dispersed phase such as the organic phase in an ACC [37]. In fact, DPEs do not follow an advection equation and they are subject to forces such as drag, lift and turbulent dispersion. For this reason, it is assumed that Lagrangian Particle Tracking (LPT) would provide a better estimation of the RTD of the dispersed organic phase compared to the advection of a passive scalar. In order to estimate the RTD using LPT, 1000 particles were injected in the domain from the organic phase inlet; these spherical particles have the same physical properties as the organic phase and a diameter equal to the time-averaged diameter of the droplets within the annulus, i.e. 0.170 mm. The transport of the particles by the continuous phase was tracked using a one-way coupled LPT solver. The RTD was evaluated following Equation (14), where the concentration of the scalar at the outlet was replaced with the count of the particles leaving the computational domain through the outlet sections. The mean residence times obtained with the three different techniques, i.e. "plug-flow", passive scalar and LPT, in both the entire system and in the mixing zone are summarized in Table 2.

The LPT-based RTD within the ACC is shown on the left hand side of Figure 14. It can be seen that the RTD obtained with the LPT is noticeably different with respect to the one obtained with the passive scalar approach (Figure 13). In particular the former distribution is wider than the latter, indicating that the standard deviation in the residence time for the particles is significantly higher compared to that of a tracer; the mean of the distribution is equal to 6.24 seconds, which is markedly higher than the mean residence team obtained with both the tracer and the plug-flow assumptions. Lastly, it can be seen that after 20 seconds of simulated time around 300 particles are still present within the system, possibly indicating the presence of dead zones in the ACC [36]. The RTD for the annular mixing region evaluated with the same LPT-based technique is shown on the right-hand side of Figure 14; also in this case the distribution appears wider with respect to the tracer-based RTD, with a significantly longer tail; the LPT-based residence time within the annulus is equal to 1.06 seconds, which is more than twice that resulting from the passive scalar calculation. The latter finding is particularly important keeping in mind that the residence time in the mixing region plays a key role in the evaluation of the mass transfer within the system, and thus using a tracer-based RTD would result in an underestimation of time available for the mass transfer process to take place within the mixing region.

Table 2. Mean residence times in the whole system and the mixing region evaluated with different techniques.

	Whole system (s)	**Mixing region only (s)**
"Plug-flow"	1.17	0.48
Passive scalar	1.19	0.49
LPT	6.24	1.06

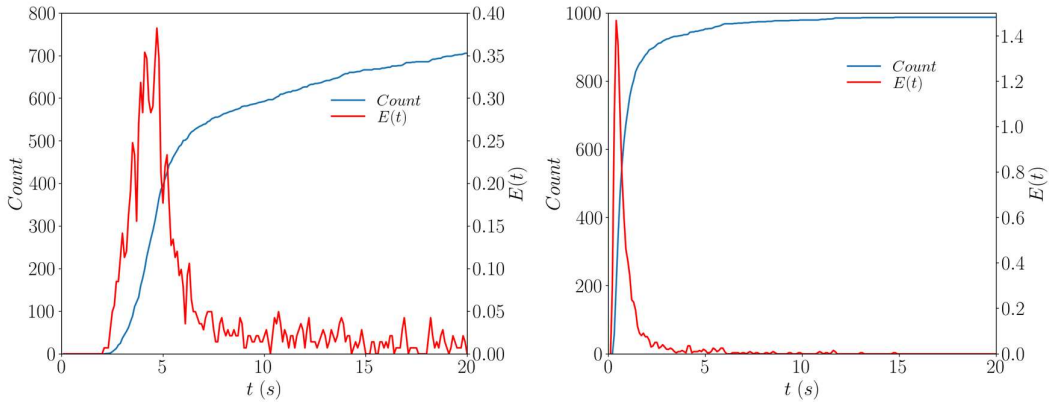

Figure 14. LPT-evaluated RTD within the entire system (left) and the mixing region (right).

3.4 Application to the prediction of mass transfer coefficients in the mixing region of the ACC

The detailed information on the hydrodynamic behaviour of the device obtained using GEMMA can be used to extract useful information on the performance of the system in terms of mass transfer.

According to the two-film theory [39], assuming infinitely fast interfacial chemistry and therefore neglecting the resistance to mass transfer at the interface, the mass transfer rate (in kg/s) from the continuous aqueous phase to the dispersed organic phase can be expressed as:

$$\dot{m} = k_{Od} A \rho_d (m Y_c - Y_d) \tag{15}$$

where A is the total interfacial area available for mass transfer, ρ_d is the density of the dispersed phase, m is the distribution coefficient of the considered system, and Y_c and Y_d are the bulk mass fractions of the solute in the continuous and dispersed phases, respectively; k_{Od} is the overall mass transfer coefficient evaluated with respect to the dispersed phase, which can be expressed as a function of the phase-specific mass transfer coefficients k_d and k_c as:

$$\frac{1}{k_{Od}\rho_d} = \frac{1}{k_d \rho_d} + \frac{m}{k_c \rho_c} \tag{16}$$

Different correlations are available in the literature to evaluate the phase-specific mass transfer coefficients k_d and k_c, which are usually expressed as a function of the Sherwood number; good reviews of such correlations are given in [40] [41]. For a given phase q the Sherwood number is expressed as:

$$Sh_q = \frac{k_q d_d}{D_q} \tag{17}$$

where k_q is the phase-specific mass transfer coefficient for phase q, d_d is the diameter of the dispersed phase and D_q is the diffusion coefficient of the solute in phase q. These correlations usually express the Sherwood number as a function of the physical properties of the fluids as well as a function of the hydrodynamic conditions within the system. For instance, the correlation from [42], suitable for evaluating the mass transfer coefficient for the continuous phase in a swarm of circulating droplets, reads:

$$k_c = \frac{D_c}{d}\left(0.725 Re_c^{0.57} Sc_c^{0.42}(1-\alpha_d)\right) \tag{18}$$

where the Schmidt number for the continuous phase is:

$$Sc_c = \frac{\mu_c}{\rho_c D_c} \tag{19}$$

and the Reynolds number is evaluated as:

$$Re_c = \frac{\rho_{d|U_r|d}}{\mu_d} \tag{20}$$

In the equations above α_d is the dispersed phase hold-up, D_c is the diffusivity of the solute in the continuous phase and $|U_r|$ is the magnitude of the relative velocity between the two phases.

Similarly, a popular correlation for the mass transfer coefficient for the dispersed phase in the case of a circulating droplet is given by [43] and reads:

$$k_d = 0.023 \frac{|U_r|}{Sc_d^{0.5}} \quad \textbf{(21)}$$

An examination of Equations (15), (18) and (21) reveals that different sets of parameters are needed for the evaluation of the mass transfer coefficients:

1. Physical and chemical properties of the system (e.g.: densities, viscosities, mass diffusivities, distribution coefficient)
2. Hydrodynamic parameters (e.g.: dispersed phase diameter, hold-up, slip velocity)
3. Interfacial area and residence time within the system, to integrate Equation (15) over time and evaluate the overall amount of extracted solute

Whilst the physical properties of the system can usually be retrieved from the literature or via ad-hoc experiments, the hydrodynamic parameters and residence time are dependent on both the characteristics of the device and on its specific operating conditions, and are very often extremely difficult to obtain experimentally, especially in the case of complex devices such as ACCs; therefore, it is evident that an accurate multiphase modelling approach for multiscale multiphase flows such as GEMMA allows the use of CFD to evaluate these key parameters needed for the evaluation of mass transfer in intensified liquid-liquid extraction devices. Within the CFD model, the mass transfer rate can be evaluated locally, based on local resolution of Equations (15), (18) and (21), with the controlling parameters evaluated on a cell-by-cells basis within the computational domain. A less computationally expensive approach is to evaluate these parameters, and hence the mass transfer performance of the system, using volume-averaged values of the variables obtained from the CFD simulation. With respect to the laboratory-scale ACC considered in Section 3.3, the simulation performed with GEMMA yields the volume-averaged values reported in Table 3 for the annular mixing region. This information, combined with knowledge of the physical and chemical properties of the system, readily allows for the evaluation of the volume-averaged mass transfer coefficients in the annular region using Equations (20) and (21), or other similar correlations available in the literature, and then for the integration of Equation (15) over time to evaluate overall mass transfer within the device. The implementation of local cell-by-cell mass transfer modelling capabilities within the GEMMA approach is foreseen for future developments of the model.

Table 3: Volume-averaged hydrodynamic parameters in the mixing region of the ACC.

Organic phase hold-up	0.335
d_{32} (m)	1.70×10^{-04}
Interfacial area A (m^2)	0.9392
Re_c	57.4828
$\|U_d\|$ ($m\ s^{-1}$)	2.4249
$\|U_r\|$ ($m\ s^{-1}$)	0.3268
Expected residence time in the annulus (s)	1.06

4. Conclusions

A novel GEneralized Multifluid Modelling Approach (GEMMA) for the simulation of multiphase flows has been applied to the simulation of the hydrodynamics of intensified liquid-liquid extraction processes, with a particular focus on Annular Centrifugal Contactors (ACCs). The GEMMA approach can seamlessly switch between multifluid formulations suitable for both large/segregated and small/dispersed interfacial scales, thus allowing for the simulation of the complex multiscale flows observed in ACCs. The switch is based on the local mesh size and flow conditions.

The simulation of the multiphase flow in the annular mixing region of an ACC has shown that the proposed approach is capable of reproducing the main features observed experimentally in such flows; it was also demonstrated that a combination of GEMMA with a reduced population balance can provide a reasonable prediction of the Sauter mean diameter of the dispersed phase, and therefore of the interfacial area density, within the system over a broad range of rotating speeds.

The simulation of a laboratory-scale ACC has been used as a proof of concept to demonstrate that GEMMA is a pragmatic approach for the simulation of the complex flow field observed in these devices; in particular, it has been shown that the modelling approach can satisfactorily predict the dispersed nature of the flow in the mixing region using a standard interface-averaging approach for small/dispersed interfaces; within the rotor region, an accurate resolution of the large/segregated interfacial morphology resulting after phase coalescence and segregation is obtained, thanks to the multifluid formulation for large interfacial scales implemented within GEMMA. The accurate resolution of the multiscale flow observed in the ACC makes available key information such as the location of the dispersion band, residence time, hold-up, droplet size distribution and interfacial area density. It is of particular interest to note that the hydrodynamic information made available by the GEMMA approach can readily be used to evaluate the overall mass transfer performance of the system.

It is concluded that the proposed modelling approach represents a useful and pragmatic tool for the simulation of intensified liquid-liquid extraction processes, which can yield valuable insights into the hydrodynamics of these processes. Future work will include further assessment of the approach and comparison with experimental observations, for which gathering of the necessary experimental data is ongoing, and the implementation of local mass transfer modelling capabilities within the GEMMA approach.

Acknowledgements

The work was supported by the EU project GENIORS (Project ID: 755171) and by the UK Department for Business, Energy and Industrial Strategy's (BEIS) through the Advanced Fuel

Cycle Programme (AFCP). The support and valuable insights from Dr. Alastair Baker are also acknowledged.

References

[1] B. Hanson, "Process engineering and design for spent nuclear fuel reprocessing and recycling plants," in *Reprocessing and Recycling of Spent Nuclear Fuel*, R. Taylor, Ed., Oxford, Woodhead Publishing, 2015, pp. 125-151.

[2] H. A. C. Mckay, "The PUREX process," in *Science and technology of tribuytl phosphate*, 1990.

[3] E. Müller, R. Berger, E. Blass, D. Sluyts and A. Pfennig, "Liquid–Liquid Extraction," in *Ullmann's Encyclopedia of Industrial Chemistry*, vol. 21, 2008, pp. 249-307.

[4] R. A. Leonard, "Design Principles and Applications of Centrifugal Contactors for Solvent Extraction," in *Ion Exchange and Solvent Extraction*, B. Moyer, Ed., Boca Raton, CRC Press, 2010, pp. 564-613.

[5] S. Vedantam and J. B. Joshi, "Annular Centrifugal Contactors — A Review," *Chemical Engineering Research and Design,* vol. 84, pp. 522-542, 2006.

[6] K. E. Wardle, "Open-Source CFD Simulations of Liquid–Liquid Flow in the Annular Centrifugal Contactor," *Separation Science and Technology,* vol. 46, pp. 2409-2417, 2011.

[7] S. Vedantam, K. E. Wardle, T. V. Tamhane, V. V. Ranade and J. B. Joshi, "CFD Simulation of Annular Centrifugal Extractors," *International Journal of Chemical Engineering,* vol. 2012, 2012.

[8] A. Prosperetti and G. Tryggvason, Computational Methods for Multiphase Flow, Cambridge: Cambridge University Press, 2007.

[9] H. Marschall, "Towards the numerical simulation of multi-scale two-phase flows," 2011.

[10] M. Sussman and E. G. Puckett, "A Coupled Level Set and Volume-of-Fluid Method for Computing 3D and Axisymmetric Incompressible Two-Phase Flows," *Journal of Computational Physics,* vol. 162, pp. 301-337, 2000.

[11] C. W. Hirt and B. D. Nichols, "Volume of fluid VOF method for the dynamics of free boundaries," *Journal of Computational Physics,* vol. 39, pp. 201-225, 1981.

[12] D. W. Theobald, B. Hanson, M. Fairweather and P. J. Heggs, "Implications of hydrodynamics on the design of pulsed sieve-plate extraction columns: A one-fluid multiphase CFD model using the volume of fluid method," *Chemical Engineering Science,* vol. 221, p. 115640, 2020.

[13] G. Cerne, S. Petelin and I. Tiselj, "Coupling of the Interface Tracking and the Two-Fluid Models for the Simulation of Incompressible Two-Phase Flow," *Journal of Computational Physics,* vol. 171, pp. 776-804, 2001.

[14] K. E. Wardle, "Hybrid multiphase CFD simulation for liquid-liquid interfacial area prediction in annular centrifugal contactors," in *Proceeding of the Global 2013*, Salt Lake City, Usa, 2013.

[15] A. De Santis, M. Colombo, B. C. Hanson and M. Fairweather, "A generalized multiphase modelling approach for multiscale flows," *Journal of Computational Physics,* vol. 436, p. 110321, 2021.

[16] The OpenFOAM Foundation, "OpenFOAM - User Guide," 2019.

[17] H. G. Weller, G. Tabor, H. Jasak and C. Fureby, "A tensorial approach to computational continuum mechanics using object-oriented techniques," *Computers in Physics,* vol. 12, pp. 620-631, 1998.

[18] E. Krepper, D. Lucas, T. Frank, H.-M. Prasser and P. J. Zwart, "The inhomogeneous MUSIG model for the simulation of polydispersed flows," *Nuclear Engineering and Design,* vol. 238, p. 1690–1702, 2008.

[19] K. E. Wardle and H. G. Weller, "Hybrid Multiphase CFD Solver for Coupled Dispersed/Segregated Flows in Liquid-Liquid Extraction," *International Journal of Chemical Engineering,* vol. 2013, pp. 1-13, 2013.

[20] J. Anez, F. Demoulin, N. Hecht and J. Reveillon, "A general purpose LES model for atomization," in *European Conference Liquid Atomization & Spray Systems*, 2016.

[21] E. Berberovic, N. P. van Hinsberg, S. Jakirlic, I. V. Roisman and C. Tropea, "Drop impact onto a liquid layer of finite thickness: Dynamics of the cavity evolution," *Physical Review E,* vol. 79, p. 036306, 2009.

[22] L. Štrubelj, I. Tiselj and B. Mavko, "Simulations of free surface flows with implementation of surface tension and interface sharpening in the two-fluid model," *International Journal of Heat and Fluid Flow,* vol. 30, p. 741–750, 2009.

[23] J. U. Brackbill, D. B. Kothe and C. Zemach, "A continuum method for modeling surface tension," *Journal of computational physics,* vol. 100, p. 335–354, 1992.

[24] J. A. Heyns and O. F. Oxtoby, "Modelling surface tension dominated multiphase flows using the VOF approach," in *6th European Conference on Computational Fluid Dynamics*, 2014.

[25] O. Ubbink, "Numerical prediction of two fluid systems with sharp interfaces," 1997.

[26] Y. Zhu, H. N. Oguz and A. Prosperetti, "On the mechanism of air entrainment by liquid jets at a free surface," *Journal of Fluid Mechanics,* vol. 404, p. 151–177, 2000.

[27] C. Drumm, M. Attarakih, M. W. Hlawitschka and H.-J. Bart, "One-Group Reduced Population Balance Model for CFD Simulation of a Pilot-Plant Extraction Column," *Industrial and Engineering Chemistry Research,* vol. 49, p. 3442–3451, 2010.

[28] M. M. Attarakih, C. Drumm and H. Bart, "Solution of the population balance equation using the sectional quadrature method of moments (SQMOM)," *Chemical Engineering Science,* vol. 64, pp. 742-752, 2009.

[29] C. Martinez-Bazan, J. L. Montanes and J. C. Lasheras, "On the breakup of an air bubble injected into a fully developed turbulent flow," *Journal of Fluid Mechanics,* vol. 401, p. 157–182, 1999.

[30] M. J. Prince and H. W. Blanch, "Bubble coalescence and break-up in air-sparged bubble columns," *AIChE Journal,* vol. 36, pp. 1485-1499, 1990.

[31] N. B. Wyatt, T. J. O'Hern and B. Shelden, "Drop-size distributions and spatial distributions in an annular centrifugal contactor," *AIChE Journal,* vol. 59, pp. 2219-2226, 2013.

[32] J. Smagorinsky, "General Circulation Experiments With the Primitive Equations," *Monthly Weather Review,* vol. 91, p. 99–164, 1963.

[33] A. Verma and K. Mahesh, "A Lagrangian subgrid-scale model with dynamic estimation of Lagrangian time scale for large eddy simulation of complex flows," *Physics of Fluids,* vol. 24, p. 085101, 2012.

[34] B. E. Launder and D. B. Spalding, "The numerical computation of turbulent flows," *Computer Methods in Applied Mechanics and Engineering,* vol. 3, pp. 269-289, 1974.

[35] P. A. Haas, "Turbulent dispersion of aqueous drops in organic liquids," *AIChE Journal,* vol. 33, pp. 987-995, 1987.

[36] B. Schuur, G. N. Kraai, J. G. M. Winkelman and H. J. Heeres, "Hydrodynamic features of centrifugal contactor separators: Experimental studies on liquid hold-up, residence time distribution, phase behavior and drop size distributions," *Chemical Engineering and Processing: Process Intensification,* vol. 55, pp. 8-19, 2012.

[37] H. S. Fogler, Elements of Chemical Reaction Engineering (4th Edition), 4 ed., Prentice Hall, 2005.

[38] P. V. Danckwerts, "Continuous flow systems: Distribution of residence times," *Chemical Engineering Science,* vol. 2, pp. 1-13, 1953.

[39] W. K. Lewis and W. G. Whitman, "Principles of Gas Absorption.," *Industrial & Engineering Chemistry,* vol. 16, pp. 1215-1220, 1924.

[40] D. Garthe, "Fluid-dynamics and mass transfer of single particles and swarm of particles in extraction columns," 2006.

[41] M. Attarakih, S. Al-Zyod, M. Abu-Khader and H. J. Bart, "PPBLAB: A New Multivariate Population Balance Environment for Particulate System Modelling and

Simulation," *Procedia Engineering,* vol. 42, pp. 1445-1462, 2012.

[42] R. R. Treybal, Liquid Extraction, McGraw Hill, 1963.

[43] G. S. Laddha and T. E. Degaleesan, Transport phenomena in liquid extraction, Tata - McGraw Hill, 1976.